Original Research Article

DFT investigation of Optoelectronic properties for $CaAO_3$ (A = Ti, Zr, and Hf)

Akeem Adekunle Adewale[1,2,6,*], AbdulRaheem Abdulganiyu[1,3,], Kamaldeen Olasunkanmi Suleman[5,***], Surajudeen Otolowo Azeez[1,5], ISMAILA TAIWO Bello[1], Yekinni Kolawole Sanusi[1,6], De Conti Claudio [2]**

[1]*Department of Pure and Applied Physics, Ladoke Akintola University of Technology, Ogbomoso, Nigeria*
[2]*São Paulo State University (UNESP), School of Engineering and Sciences, 19274-000 Rosana, SP, Brazil.*
[3]*Department of Physics and Materials Science, Kwara State University, Malete, Nigeria.*
[4]*Department of Physics, Nigeria Maritime University, Okerenkoko, Warri, Nigeria.*
[5]*Department of Physical and Chemical Sciences, Federal University of Health Sciences, Ila- Orangun, Nigeria;*
[6]*Nanotechnology Research Group (NANO+), Ladoke Akintola University of Technology, Ogbomoso, Nigeria*

Use yor device to scan and read the article online

Citation A.A. Adewale , A. Abdulganiyu, K.O. Suleman, S.O. Azeez, I.T. Bello, Y.K. Sanusi, D.C. Claudio. DFT investigation of Optoelectronic properties for $CaAO_3$ (A = Ti, Zr, and Hf). *J. Eng. Ind. Res.* **2025**, * (*):**-**.

https://doi.org/ 10.48309/JEIRES.2025.531051.1247

CC BY

Article info:
Submitted: 2025-06-28
Revised: 2025-07-21
Accepted: 2024-**-**
ID: JEIRES-2506-1247

Keywords:
Perovskites; Absorption spectra; Optoelectronic devices; PBE; Refractive index.

ABSTRACT

In recent times, the synthesis and simulation of perovskite materials have gained significant interest in renewable energy. The diverse metal-halide perovskites are very useful in optoelectronic devices. However, lead-based perovskites are toxic, unstable, and vulnerable to degradation when exposed to high temperatures, and their instability is the major restriction for their commercial use. This research paper centered on the first-principles calculations of structural and optoelectronic features of $CaAO_3$ (A = Ti, Zr, and Hf) by employing the Generalized Gradient Approximation (GGA) Perdew-Burke-Ernzerhof (PBE), and DFT+TB-mBJ exchange-correlation functional. The calculations of the electronic properties revealed that the $CaAO_3$ (A = Ti, Zr, Hf) has indirect and direct band gaps. To treat the electron-electron interactions, we utilized the PBE exchange-correlation functional, which revealed non-phonon-assisted energy gaps of 2.5 eV, 3.51 eV, and 3.70 eV, and phonon-assisted energy gaps of 1.88 eV, 3.21 eV, and 3.64 eV for $CaAO_3$ (A = Ti, Zr, and Hf), respectively. These values are consistent with the reported theoretical literature. By employing the DFT+mBJ exchange-correlation functional, the direct band gaps (non-phonon-assisted) of 3.21 eV, 4.70 eV, and 5.21 eV and indirect band gaps (phonon-assisted) of 2.73 eV, 4.24 eV, and 5.03 eV were obtained, which are in excellent agreement with the limited experimental values reported, though with slight underestimation. Moreover, the optical absorption spectra, dielectric constants, and refractive index calculations testify to their applications in optoelectronic devices.

***Corresponding Author: Akeem Adekunle Adewale** (aaadewale38@lautech.edu.ng); **AbdulRaheem Abdulganiyu** (abdulraheem.abdulganiyu@kwasu.edu.ng); **Kamaldeen Olasunkanmi Suleman**(talk2dprof@gmail.com)

Introduction

With the incessant increase in industries and global population, there is a high demand for energy, and the tendency for this request to increase is escalating hysterically [1]. The concern is not only from the energy-demanding factor and its crisis, but also on the environmental challenges posed to the surroundings that need to be remediated due to the rapid consumption of the most commonly used fossil fuels [2-4]. Moreover, the consumption of fossil fuels is faster than it can be replenished, and their massive impact and contribution to escalating issue of environmental pollution due to the presence of heavy toxic metals and harmful gases released during their combustion into the environment [5]. Due to these deficiencies, there is a need for a stable, nontoxic, inexhaustible, and environmentally friendly substitution for fossil fuels with the development of effective materials that can harness a vast region of the solar spectrum. Perovskite materials have attracted much attention in this regard and the application of renewable energy because of their diverse applications and uses in variable-frequency capacitors [6], microwave technology, field devices, sensors, optoelectronic, superconductivity, ferroelectricity, thermoelectric devices, and many more [6-10].

The extensively studied metal halide perovskite material with the general formula ABX_3 (where A and B atoms are organo-inorganic cations, respectively, with X halide anion) is not stable, and it is toxic due to the presence of lead (Pb^{2+}), which oxidizes when exposed to air. In recent years, calcium titanate ($CaTiO_3$), a multi-inorganic oxide, has garnered a significant extent of attention from researchers due to its inexpensiveness, low toxicity, high chemical stability, strong catalytic activities, easy synthesis, and optimal band edge position [6]. It is an alkaline earth titanate like $BaTiO_3$ and $SrTiO_3$. Its application as ferroelectric, electro-conductive, photorefractive, and photovoltaic materials have attracted the attention of researchers, and the cubic phase $ATiO_3$ is commonly used in the microelectronics industry, such as in piezoelectric actuators, spintronics, integrated circuits, active and passive devices [8], and many more.

It is known that some properties, such as the electrical and optical properties of materials are largely determined by their electronic structure of materials. Therefore, understanding their electronic structure is pertinent to improving these functions for their new technological applications [11,12]. The consistent calcium titanate ($CaTiO_3$) of the space group Pm-3m, belongs to the class of paraelectric materials that do not exhibit spontaneous electric polarization unless it is polarized by an external electric field [6].

In the past, the optoelectronic features of ferroelectric $CaTiO_3$ have been studied through first-principles calculations using the GGA-PBE exchange-correlation functional. The calculation was conducted within the range of 0-100 GPa. While the band gap remained direct with a gradual increase in value, a decrease in lattice parameters which was attributed to the increase in pressure, was reported [13]. In another work, the correlation of structural, electronic, and optical properties of Ce-doped $BaTiO_3$ was investigated using the first principles. Here, authors reported a reduction in the band gap which they attributed to the substitution of Ce as the movement of both the valence and conduction bands was induced, which is invariably constituting to the increase in electrical conductivity [14]. Ghazanfar *et. al* employed the use of full-potential linearized augmented plane wave and plane wave pseudopotential methods to study the structural and optoelectronic properties of ferroelectric $CaTiO_3$ (with the space group Pbnm) and use generalized gradient approximation to treat the exchange-correlation functional. They performed an analytical review of the electronic and optical properties of bulk and slab $CaTiO_3$:Eu^{2+} using the density functional theory method [8]. Tahiri *et. al* performed calculations on structural and optoelectronic properties of $Ba_{1-x}Ca_xTiO_3$ and $Ba_{1-x}Sr_xTiO_3$ (x = 0.4, 0.6) within the DFT framework using GGA approximation as implemented in the ABINIT package. They reported an increase in band gap as the concentrations of Ca and Sr increased [15].

In the literature, we observed that many of the published reports centered on the orthorhombic

structure $CaTiO_3$ and substitution of the A-site, with little research on the substitution of the B-site, limited works of literature on the cubic structure of $CaTiO_3$, a report on $CaZrO_3$, and no research work on comparing the contribution effect of the B-site. Based on the current literature, experimental and theoretical calculations on the $CaHfO_3$ compound have not been explored. Therefore, in this research work, we employed the use of density functional theory to calculate the elastic, thermal, and optoelectronic properties of a cubic ABO_3 (A= Ca, B=Ti, Zr, and Hf) using the PBE-sol and meta-GGA exchange-correlation functional implemented in the Wien2K code [16].

Computational details

In this study, we have employed the first principles FP-LAPW [17] method to investigate the elastic and optoelectronic properties of $CaAO_3$ (A=Ti, Zr, and Hf) within the framework of Density Functional Theory (DFT), utilizing flavors of GGA [18] and meta-GGA [19] exchange-correlation functionals implemented in Wien2K code [16]. In the calculations, approximations were treated using the valence electrons of the electronic configurations for the compounds under study as follows: $[Ar]4s^2$, $[Ar]3d^24s^2$, $[Kr]4d^25s^2$, $[Xe]4f^{14}5d^26s^2$ and $2s^22p^4$ for Ca, Ti, Zr, Hf and O, respectively, with Ar, Kr, and Xe representing the electronic configurations of Argon, Zirconium and Xenon. To accommodate to the maximum spatial frequency of the electronic wave function (plane wave cutoff), we set $K_{max} = 10/R_{MT}$ in the plane waves, where the parameter R_{MT} functions as the magnitude of the atomic sphere in a given system and this expansion parameters has a significant effect in the calculation speed of the simulation. The degree of convergence is achieved using the relation $R_{MT}\ K_{max} = 10$. To achieve self-consistency, the integration of the k-space in the irreducible Brillouin Zone (IBZ) is chosen to be 18 k-points in a grid of 8×8×8 meshes, which is equivalent to 512 k-points in the full Brillouin zone. -8.0 Ry of energy spaces the central part and the valence electrons with the enlarged scattering of electrons within the muffin-tin spheres, controlled and catered for by setting Fourier expansion Gmax = 14 $(a.u.)^{-1}$. Moreover, it's not a new trend that first principle DFT calculations using GGA-PBE often underestimate the band gap because the excited states are not considered, and the DFT+mbj technique helps to subdue and improve on the problem of underestimation and provide an agreement with the experimental value. However, in all these approximations, the k-vector often maintains its initial position of phonon transition, and the nature of the band gaps usually remains invariant in all respects.

Results and Discussion

Geometry optimization

The structural properties of the understudied materials are recorded at ambient temperature and pressure. This is achieved by running self-consistent field calculations using Birch Murnaghan's equation of state [20] given by the expression in Equation (1) [11]. To study the structural stability of these perovskite materials, the volume optimization of the unit cell was conducted to achieve the optimized or minimal values for the bulk modulus (B_0), bulk modulus derivative (B'_0), lattice parameter (a_0), minimum volume (V_0) and the ground state energy (E_0) with the convergence tolerance limit set to 10^{-5} Ry at ground state energy. Our results are compared with the relevant available literature. Figure 1 shows the fittings of total energy against the individual compound volumes. The optimized convergence values at 0 GPa are recorded in Table 1. The computed data for this present work are those without citation in Table 1 using GGA-PBE and DFT+mbj functionals [6]. We performed the calculation using GGA-PBE functional [8], utilized GGA+U to account for the interaction between electrons [15], computed the structural parameters using GGA-PBE [5]. Previously, structural calculations were conducted with the flavor of GGA-PBEsol method, when investigating the structural and electronic properties of pressure-dependent cubic $CaTi0_3$ using GGA and GGA+U [21] functionals, while the experimental results obtained by other researchers [14,22,23] are tabulated respectively alongside some theoretical data from literature. It was observed that the optimization of the cubic $CaTi0_3$, $CaZr0_3$,

and $CaHf0_3$ structures is in good agreement with both theoretical and experimental values, exhibiting small deviations, as shown in Table 1. Moreover, there is a reduction in the lattice constants as the ionic radii of the B site decrease, which leads to a decrease in atomic size, and this is in line with the literature [9,15,24].

$$P = \frac{B}{B'}\left[\left(\frac{V_o}{V}\right)^{B'} - 1\right] \quad (1)$$

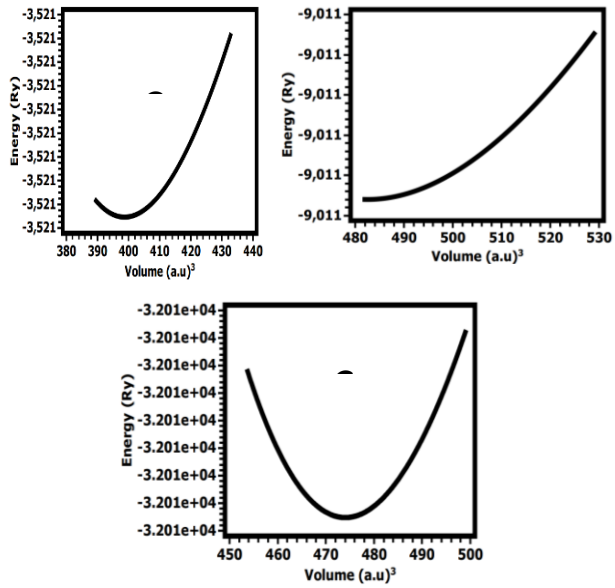

Figure 1: Variation of energy (Ry) against the volume (a.u)³ of the $CaAO_3$ (A=Ca, Zr, and Hf) perovskite compounds

Table 1: The calculated lattice constant, bulk modulus, bulk modulus derivative, minimum volume, and ground state energy

Parameter		Compounds		
		$CaTiO_3$	**$CaZrO_3$**	**$CaHfO_3$**
Lattice constant (Å)	The present work	3.8948	4.1506	4.1261
	others	3.882 [11] 3.856 [9]		
Bulk modulus (GPa)	The present work	183.3642	162.1982	165.9078
	others	176.20 [8,18], 200.598 (189.61) [9]		
Bulk modulus derivative (B')	The present work	5.1829	4.9258	4.5319
	others	5.046 [9]		
Minimum volume (V_0) in (a.u)³	The present work	398.7209	482.5244	474.0381
	others	395.26 [11], 386.846 [9]		
Ground state energy (E_0) in Ry	The present work	-3520.67	-9011.482979	-32008.742523
	others	-3520.67 [21]		

Electronic band structure

The comprehension of the uniqueness of the electronic band structure of materials leads to their variation and adaptation in a wide range of notable applications in electronics and optoelectronic devices. The band theory typically explains how various electrons of each atom behave and how the energy levels of each atom overlap in a continuous way to form energy bands. The energy difference between the top of the valence band and the bottom of the conduction band is known as the energy band gap, which informs us about the conductivity of materials [6,8]. The energy band gap is a fundamental concept in materials science and engineering that distinguishes different materials and classifies them into metals and semi-metals, semiconductors, and insulators. If both bands overlap, the energy gap (E_g) is zero, or the energy band gap is relatively small, the material is metallic. However, if the energy difference between the valence band minimum and the conduction band maximum is large enough or greater than 3 eV, the solid is an insulator, and if E_g is within the range of $0 < E_g < 3$ eV, it is a semiconductor material [6]. Understanding of the band structure provides vital information about the occupied and unoccupied regions of electrons in solids and the transition of electrons between the bands. The nature of the electron transition could be phonon-assisted or not. If the k-vectors between the transitions of electrons from the filled band to the empty band are directed along the same path length, it is a direct band gap, otherwise, it is an indirect energy gap [8].

The energy band structure diagrams of the studied perovskite materials using two different types of exchange-correlation functionals are depicted in Figure 2. The calculated energy gaps are presented, as shown in Table 2. Based on Figure 2, the faint black line marked at 0 eV represents the Fermi energy level. From Figure 2(a, b, and c), the calculated direct energy gap (E_g) values with GGA-PBE x-c functional under standard atmospheric conditions for the cubic $CaTiO_3$, $CaZrO_3$, and $CaHfO_3$ are 2.30 eV, 3.51 eV, and 3.70 eV, respectively, and indirect band data are also tabulated. The values of the band gaps exhibit a small deviation from the reported theoretical data. From this present work, the non-phonon assisted E_g of $CaTiO_3$ is 2.30 eV which is very close to 2.409 eV [6] and 2.40(2.55) eV [14] calculated by Guo *et al.* and Boudali *et al.* using a plane wave pseudopotential method and all electron calculation, respectively, slightly higher compared to the plane wave method with GGA functional that resulted to a value of 2.20 eV [25] by Zhu *et al.* Moreover, Tahir *et al.* investigated the electronic and optical properties of Ba and Sr-doped perovskite using the plane wave method under GGA with Fritz-Haber-Institute (FHI) pseudopotentials, and they obtained a value of 2.433 eV [15]. Ghazanfar *et al.* performed a first principle calculation using an all-electron full-potential linearized augmented plane wave method with the GGA+U method to obtain a band gap result of 2.839 eV [8]. Our DFT calculations' indirect band gap value of 1.88 eV agrees with the reported theoretical values of 1.90 eV [11] 1.89 eV [9], and 2.003 eV [21] obtained by Kamruzzaman *et al.*, Adewale *et al.*, and Tariq *et al.*, with a percentage deviations of ≈1.053, ≈0.529, and ≈6.14, respectively.

However, our calculated values are lower when compared to the experimental values of 3.70 eV [26], 3.50 eV [27], 3.62 eV [24] and 3.51 eV [28] calculated by Boutinaud *et al.*, Ueda *et al.*, Minagawa *et al.*, and Rosa *et al.*, respectively. The underestimation of E_g is due to the GGA functional not including the excited states, and this can be addressed for by using the scissors method sometimes, extensions of GGA and LDA, or meta-GGA exchange-correlation functionals [6,21,29].

To address to the underestimation of the energy band gap, we performed DFT+mbj calculations, and the results are summarized in Table 2. For $CaTiO_3$, our calculations showed that the meta-GGA approach improved the underestimated results of the energy band gap with percentage deviations of 13.24 when compared to [26], 11.33 when compared to [24], and 8.29 when compared to [27], respectively, for the direct k path using meta-GGA. Furthermore, the calculated data obtained for the indirect k path using DFT+mbj is in good agreement with the reported values, as presented in Table 2, with a small percentage deviation. These variations may be attributed to low value of k-point

sampling, strong correlations of the metal oxides present, the complexity of the electronic structure, and various other factors. The indirect k-point band gap obtained from our calculations using the DFT+mbj method for compounds studied, particularly for $CaTiO_3$ and $CaZrO_3$, the calculated data is in good agreement with the reported literature as tabulated in Table 2, and the band structures are similar when compared to the previously reported works [11,21].

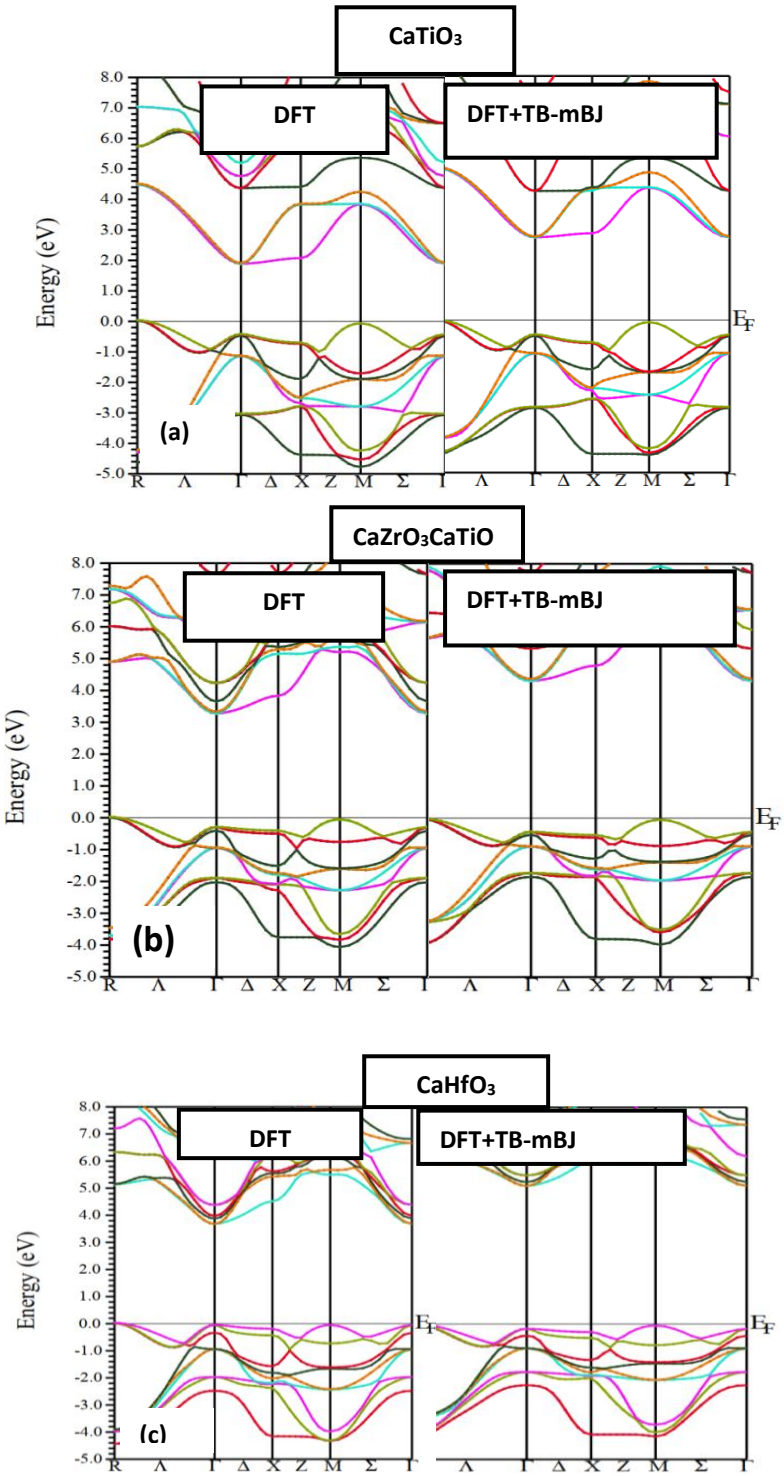

Figure 2: Energy band structure for the materials studied along the high symmetry point in the Brillouin zone using GGA-PBE and TB-mBJ exchange-correlation functional

Table 2: Tabulated energy band gap for the understudied materials using GGA-PBE and TB-mBJ exchange-correlation functional

Samples Bandgap (eV)		DFT		DFT + TB-mBJ	
		G-G	**G-R**	**G-G**	**G-R**
$CaTiO_3$	Present work	2.30	1.88	3.21	2.73
	others	2.409 [6], 2.40 [14], 2.20 [25], 2.433 [15], 2.839 [8], 2.36 [9], 2.45 [30]	2.003 [21], 1.90 [11], 1.89 [9], 1.50 [12]	3.70 [26]^{exp}, 3.50 [27]^{exp}, 3.62 [24]^{exp}, 3.29, 4.38 [30], 2.55 [14]	2.780 [31], 2.82 [9], 3.80 [30]
$CaZrO_3$	Present work	3.51	3.21	4.70	4.24
	others	3.74 [30]	5.5 [30]^{exp}	6.23 [28], 5.7 [28]^{exp}, 4.93 [32]	
$CaHfO_3$	Present work	3.70	3.64	5.21	5.03
	others	4.37 [30]	6.1 [30]^{exp}		

Density of states

To have a distinct picture of the structure of solids, the density of states remains one of the vital parameters that depict the contributions of the atomic orbitals at each level. It enables the comprehensive understanding of results [4,8]. The DOS, often represented as $\rho(E)$, is defined as the number of states within a given energy range [33]. It is expressed mathematically as Equation (2):

$$\rho(E) = \frac{dN}{dE} \tag{2}$$

Where, E denotes the energy and dN represents the number of states within a small energy range dE.

DOS provides insightful information about the band structure of materials and the orbital interactions within ranges of energy levels. Moreover, the contributions of each atomic orbital in both the valence and the conduction bands are revealed through the DOS [11], and the gap between the two bands indicates the value of the energy band gap. DOS has become an indispensable parameter in the history of the electronic structure of materials, and its applications in physics and engineering cannot be overstated. Therefore, it is impossible to

discuss certain properties of materials without addressing the significant roles and impact the DOS plays [4,28].

There are various types of DOS, such as total DOS, partial DOS, local DOS, projected DOS, and many more. Any of these can be used to account for desirable information about the structure of the materials being under consideration. However, we only discuss in this article, two (2) major categories of density of states, namely Partial Density of States (PDOS) and Total Density of States (TDOS) [8,34,35]. Using TDOS and PDOS, all relevant properties about the atomic spins and their specific contributions to the band structure can be achieved [15].

All the crystals used for our calculations at 0 GPa are cubic structures with the general formula $CaAO_3$ (A=Ti, Zr, and Hf). Figure 3 (a, b, and c) depicts the structures for both total and partial density of states for the $CaTiO_3$, $CaZrO_3$, and $CaHfO_3$ compounds, which are consistent when compared to the literature [4,6,18]. The Fermi level is represented by the vertical dark dotted lines passing through the spins of electrons, separating both the valence and conduction bands. From Figure 3(a, b, and c), the TDOS shows the effective contributions of the spin-up and spin-down of atoms in the compounds. Moreover, the PDOS shows specific atomic orbital contributions of each atom to TDOS. From Figure 3(a), moving away from the Fermi energy, the contributions from the (s and d) are observed, along with the p orbitals of Ti and O atoms, together with the p orbital of Ti atoms in the valence band, respectively. Additionally, moving away from the conduction band, we observe the contributions of the d and p orbitals of Ti and O atoms, some contributions from the p orbitals of Ca and Ti atoms, and contributions from the s orbital of O atoms. Besides the Fermi energy, Ti-d, O-s, and O-p orbitals have a significant contributions for both bands and the mixing of Ti-d, O-s, and O-p orbitals, which is correlated with the literature [4,12].To reinforce these orbitals' contribution, the DOS peaks observed at -4.375 eV, -4.402 eV, and -1.055 eV are corresponding values for Ti-3d, Ti-4s, and O-2p orbitals, respectively. This shows the strong confinement of orbitals at the regions. From Figure 3(b), moving away from the Fermi energy, there are contributions of (s and d) and p orbitals of Zr and O atoms, along with the p orbital of Zr atoms in the valence band, respectively. Additionally, moving away from the conduction band, we observe the contributions of the d and p orbitals of Zr and O atoms, some contributions from the s orbitals of Ca and O atoms, and contributions from the p orbital of Zr atoms. Besides the Fermi energy, both bands are primarily contributed by Zr-p, Zr-d, O-s, and O-p orbitals, along with the mixing of Ca-s, Zr-p, and O-s orbitals, which agree well with relevant previous works [4,12]. To further explain the orbitals' contribution, the DOS peaks observed at -3.747 eV, -3.557 eV, and -0.781 eV correspond to values for Zr-4d, Zr-5s, and O-2p orbitals, respectively, indicating a strong confinement of orbitals in the region. From Figure 3(c), moving away from the Fermi energy, there are contributions of (s, p, and d) and p orbitals of Hf and O atoms, along with the s orbital of Ca, p orbital of Hf atoms in the valence band, respectively. Additionally, moving away from the conduction band, we observed the contributions of the d and p orbitals of Hf and O atoms, some contributions from the s and p orbitals of Ca and f orbitals of Hf atoms, and contributions from the s orbital of O atoms. Beyond the Fermi energy, both bands are primarily contributed by Hf-s, Hf-d, Hf-f, O-s, and O-p orbitals and the hybridization of Hf-d, O-s, and O-p orbitals, which aligns with previous research [4,12]. To reinforce these orbitals' contribution, the DOS peaks observed at -3.945 eV, -4.163 eV, and -0.7611 eV correspond to values for Hf-5d, Hf-6s, and O-2p orbitals, respectively. This demonstrates the concentration of orbitals in the region. In conclusion, it is evident that the band structure largely consists of the contribution of O-2p and Ti-3d states for $CaTiO_3$, O-2p and Zr-4d states for $CaZrO_3$, and O-2p and Hf-5d states for $CaHfO_3$. This indicates that Ti, Zr, Hf, and O atoms significantly influence the energy band gaps of the studied compounds.

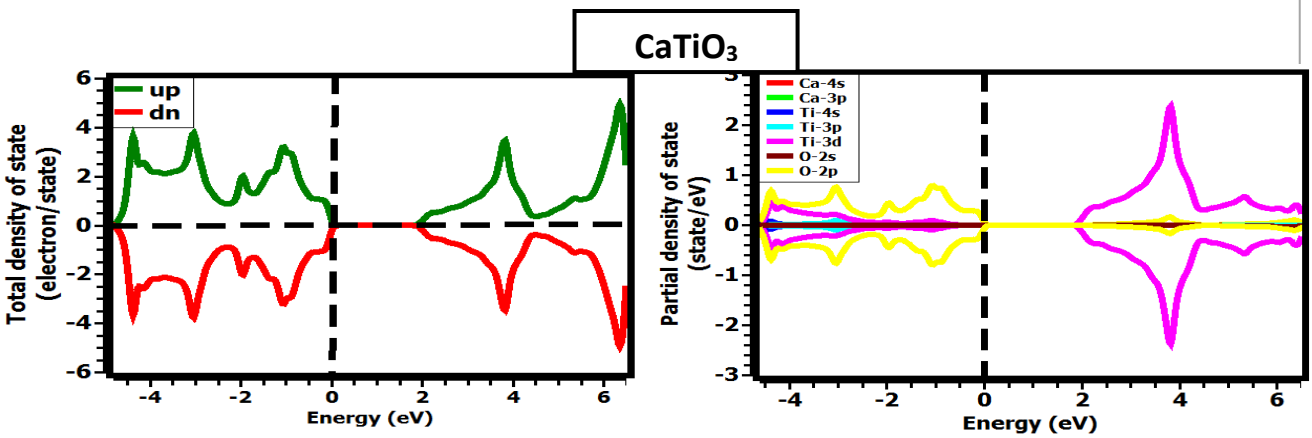

Figure 3a: Total density of state (TDOS) and partial density of state (PDOS) of cubic $CaTiO_3$

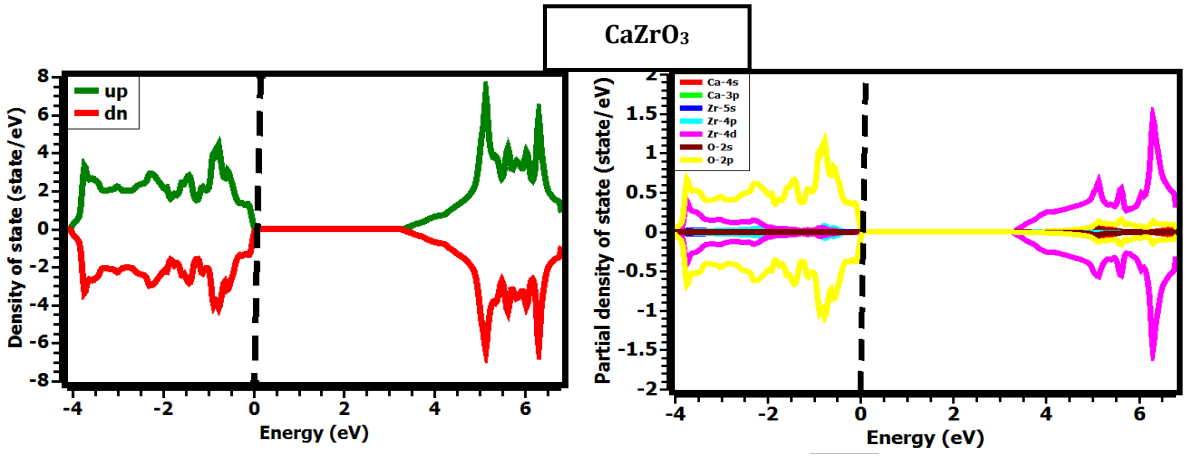

Figure 3b: Total density of state (TDOS) and partial density of state (PDOS) of cubic $CaZrO_3$

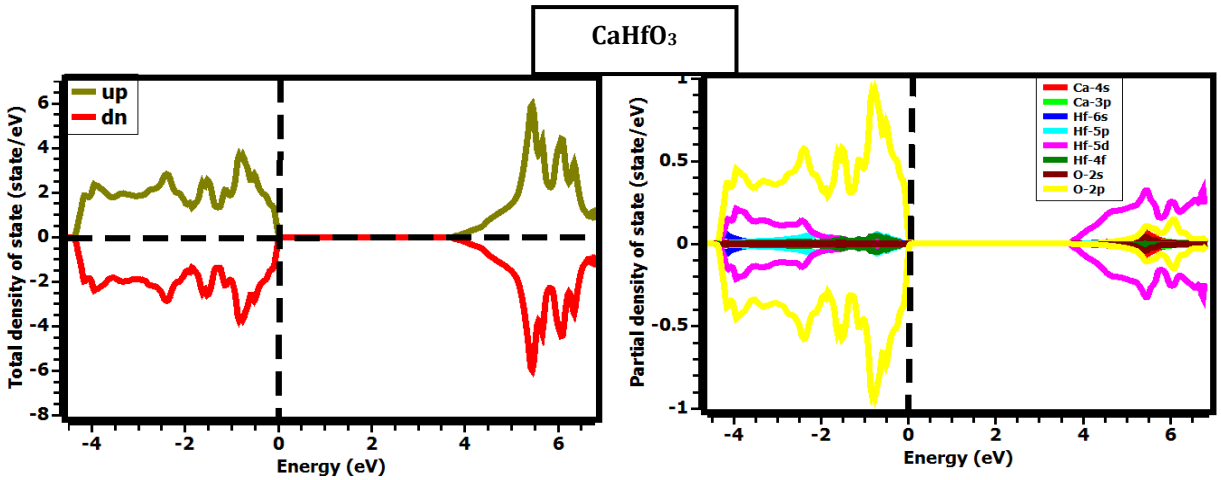

Figure 3c: Total density of state (TDOS) and partial density of state (PDOS) of cubic $CaHfO_3$

Optical properties

One of the crucial criteria that characterize behaviors and the response of materials to the incident electromagnetic radiation is unveiled through the calculation of optical properties [6,30]. The information from the optical calculations can be linked to the band structures of materials. From this work, the major calculations reveal the dielectric function, absorption coefficient, optical conductivity, energy loss function, reflectivity, refractive index, and extinction coefficient. An intense optical absorption and considerable dielectric constants are vital for selecting optoelectronic devices [36]. The real ε_1 and the imaginary ε_2 form the complex dielectric function for the three compounds as shown in Figure 4(a), respectively.

It can be seen from Figure 4(a) that the $\varepsilon_1(0)$ of the cubic structure for the three compounds $CaAO_3$ (A=Ti, Zr, and Hf) corresponds to 5.81, 4.36, and 4.10 at 0 GPa, respectively. Moreover, the bent shape distribution of ε_2 is due to the transition of electrons between energy bands. This is substantiated in the orbital contribution of the density of states, as shown in Figure 3(c). At zero pressure, two major peaks are observed in the plots of imaginary dielectric part for the studied compounds $CaBO_3$ (B=Ti, Zr, and Hf) and these peaks are 4.3402 eV and 6.7892 eV, 5.4015 eV and 8.3947 eV, and 5.6736 eV, 8.1498 eV, and 10.8982 eV, respectively. These peaks arise from the transition of O-p atomic orbitals and Ti–d orbitals to unoccupied Ti–p orbitals for $CaTiO_3$. It follows the same orbital contributions as the other two compounds. As the B site is substituted, there is a shift in the trend of the imaginary dielectric function to higher energies. This indicates an increase in the transition energy for these compounds; thereby, the energy band gap increases. This is consistent with the results calculated for band structures, as E_g ($CaTiO_3$) < E_g ($CaZrO_3$) < E_g ($CaHfO_3$) in Table 2. The computed static dielectric constant $\varepsilon_1(0)$, refractive index η (0), and reflectivity spectra $R(0)$ are shown in Table 3 below, with a few literature data reported.

Figure 4(b1) shows the calculated absorption coefficient against the photon energy of the three compounds. The absorption edges recorded from the calculation using GGA-PBE are 3.28 (2.408 eV), 3.35 (4.041 eV), and 3.10 (3.742 eV) for Ti, Hf, and Zr compounds, respectively, corresponding to the shifting of electrons from the valence band to the conduction band at the Γ point. These values correspond to the optical band gaps and are in the range of the reported literature, but the calculated electronic band gaps in this work are slightly underestimated. The calculated values of the absorption coefficient above indicate that the titanium compound has a higher absorption and will absorb more of the incident energy that falls on it when compared to the other studied compounds. It is observed that there is a small fraction of absorption in the visible region of 1.24-3.26 eV, while the ultraviolet region occupies a larger portion of the absorption spectra. Moreover, due to the transition of electrons, the absorption grows as the energy shifts towards the right side and decreases between 19 eV and 25 eV. These materials are semiconductors with direct/indirect optical band gaps. The onset of absorption corresponds to the valence-to-conduction band transitions at high symmetry points in the Brillouin zone. The Ti compound showing the highest absorption, implies better photon–electron coupling and stronger light–matter interaction. The strong absorption observed in the UV region suggests that the studied materials are UV-absorbing and could be optically transparent in the visible range, depending on thickness.

The optical reflectivity of the cubic $CaBO_3$ (B = Ti, Hf, and Zr) is depicted in Figure 4(c1). In the visible region of 1.24 eV to 3.26 eV, at 0 GPa, the reflectivity is in the range of 0.115 - 0.171 for the studied materials. From this value range, it is observed that the materials under investigation possess non-metallic lusters due to their low reflectivity (R), which is less than 30 % in the visible spectrum [4]. As the B-site is replaced, the value of reflectivity increases as follows: Hf < Zr < Ti. Guo *et al.* reported that materials are

categorized as a metallic luster when R > 0.25 and a strong metallic luster when R > 0.5 [6]. Therefore, at 0 GPa, it can be concluded that the studied materials exhibit semiconductor properties. $CaTiO_3$, having the highest R, is still within the semiconductor class but is closer to the metallic side than the others.

Figure 4(c2) displays the refractive index against photon energy between 0 and 25 eV. At zero frequency, the η (0) values are 2.41, 2.02, and 2.09 for Ti, Hf, and Zr compounds, respectively. Based on this figure, there is an increase in the refractive spectra to their respective maxima of 3.02 at 2.762 eV for Ti, 3.04 at 5.456 eV for Hf, and 3.09 at 5.157 eV for Zr materials, which then decreases to the values 0.482, 0.275 and 0.633 at energy levels of 11.4696 eV, 17.53774 eV and 11.49681 eV, respectively. Moreover, for promising optical materials and applications, the refractive index falls in the effective range between 0 and 1 in the visible and ultraviolet regions, and this calculation shows that all materials studied are suitable for optoelectronic devices. To substantiate this, there is a similar trend in the curves between the η and ε_1, and an inverse relationship exists between the two spectra as depicted in their respective curves.

The energy dissipated due to the interaction of fast-moving electrons within materials is calculated by plotting the energy loss function against the photon energy. This plot displays inter- and intra-band transitions of electrons [8]. Figure 4(d1) represents the loss function of the studied compounds within the optical radiation region. This figure shows that as the B-site is replaced, the value of the energy loss function changes and in an increasing order of 0.00126, 0.00130, and 0.00142 for Hf, Zr, and Ti, respectively. These values demonstrate a direct correlation with the absorption coefficients of each compound within the visible region, and there is an inverse relationship between the energy loss function and the refractive index. The refractive index is minimized at the maximum energy loss function and vice versa. However, there is a direct relationship between the energy loss function and the absorption coefficient, as shown in Figure 4(d1) [4,6,26].

Figure 4(d2) displays the attenuation energy of the three compounds. It exhibits how the extinction coefficient k (ω) varied with the photon energy. It displays a uniform value between 0 eV and the optical edge value, and it then increases. The maximum values obtained for the three compounds are 1.70, 1.84, and 1.79 for Hf, Zr, and Ti, respectively. It is pertinent to note that $\varepsilon_2(0)$ of the absorption coefficient gives the extinction coefficient, which indicates a relationship between the two parameters, but they are not directly related. The high values of $k(\omega)$, especially in the visible and UV range, suggest strong optical attenuation, with $CaTiO_3$ and $CaZrO_3$ optically more absorbing than $CaHfO_3$.

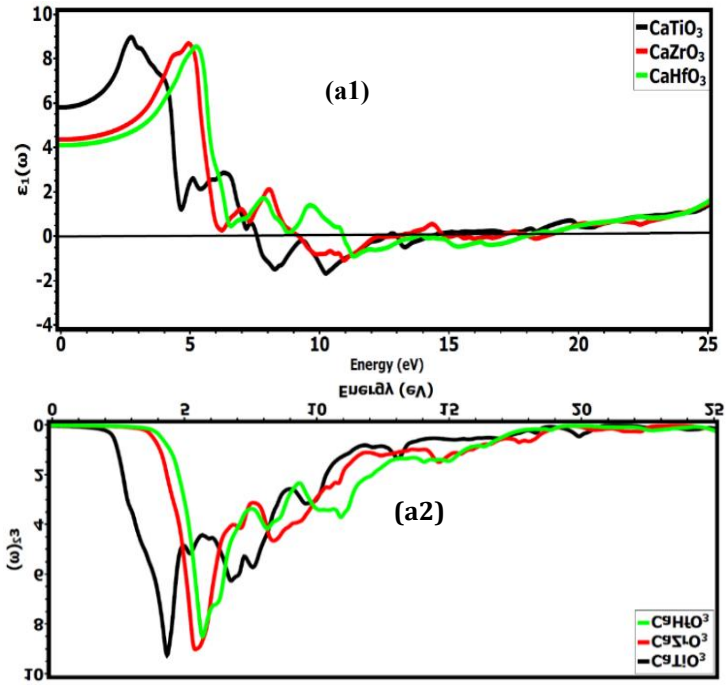

Figure 4a: Calculated ε_1 and ε_2 of the dielectric function for the $CaAO_3$ (A=Ca, Zr, and Hf) perovskite compounds

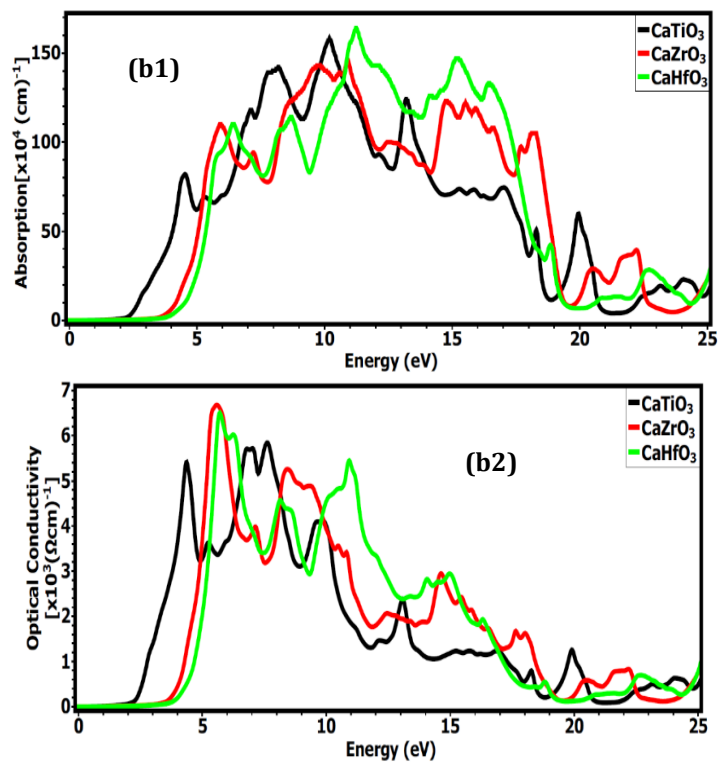

Figure 4b: The absorption spectra and optical conductivity for the $CaAO_3$ (A=Ca, Zr, and Hf) perovskite compounds

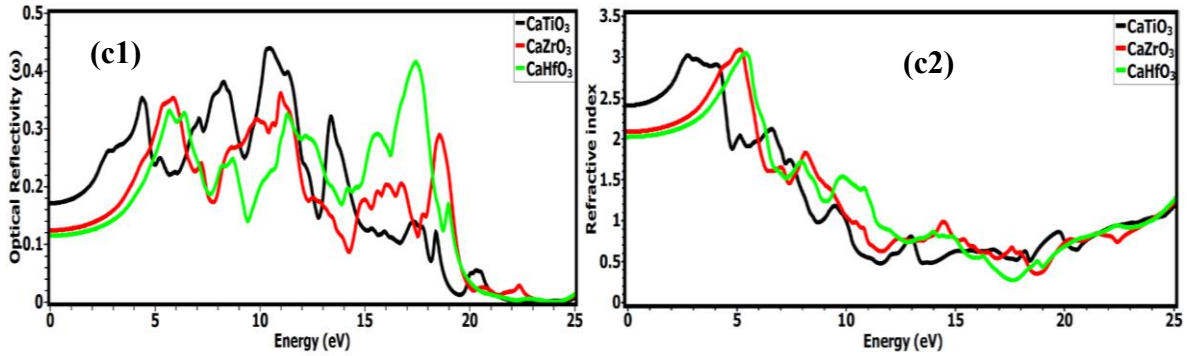

Figure 4c: Optical reflectivity (ω) and refractive index (ω) for the $CaAO_3$ (A=Ca, Zr, and Hf) perovskite compounds

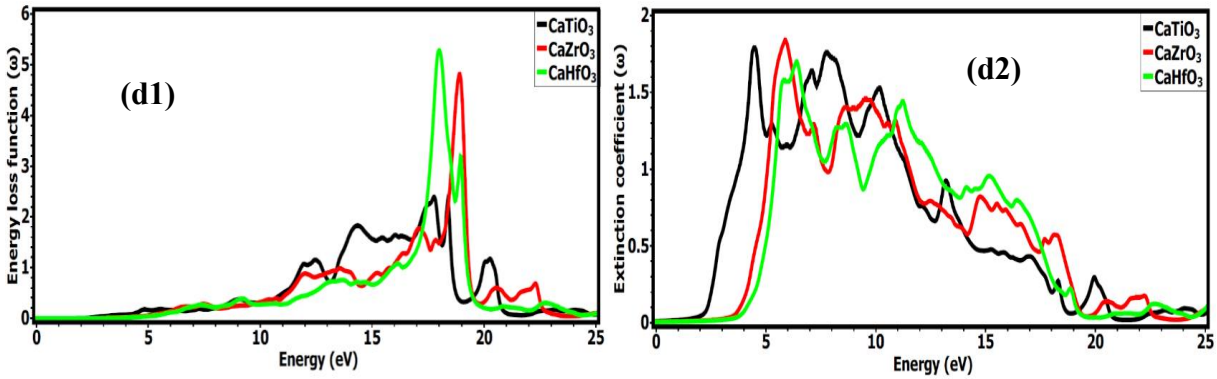

Figure 4d: Energy loss function (ω) and the extinction coefficient (ω) for the $CaAO_3$ (A=Ca, Zr, and Hf) perovskite compounds

Table 3: The computed static dielectric constant, refractive index, reflectivity, and absorption for the studied compounds using GGA-PBE exchange-correlation functional

Compound	$\varepsilon_1(0)$	$\eta(0)$	$R(0)$	$\alpha(0)$
$CaTiO_3$	5.81, 6.25 [11], 6.347 [6]	2.41, 2.47 [11]	17.1%	0.001370
$CaHfO_3$	4.10	2.02	11.5%	0.000723
$CaZrO_3$	4.36	2.09	12.4%	0.000816

Conclusion

This work presents the structural and optoelectronic properties of $CaAO_3$ (A = Ti, Zr, and Hf) based on the Density Functional Theory (DFT). Considering the Goldschmidt tolerance and octahedral factors, all the compounds crystallize into cubic structures with the values of 0.967 and 0.432 for $CaTiO_3$, 0.913 and 0.514 for $CaZrO_3$, and 0.917 and 0.507 for $CaHfO_3$, respectively. Our calculations revealed that the valence and conduction bands occur at different k-points, making the samples an indirect bandgap materials. The calculated band gaps agree well with both the theoretical and experimental data reported. Collectively, these findings confirm that all three compounds are semiconductors with promising optical characteristics. $CaTiO_3$ emerges as the most optically active, making it the best candidate for

UV-Visible light-harvesting applications, such as solar absorbers, photodetectors, and light-emitting diodes. Meanwhile, the $CaHfO_3$, with its lower absorption and reflectivity, may serve better in applications requiring higher transparency and lower optical loss.

Acknowledgments

The authors would like to acknowledge financial support from the Tertiary Education Trust Fund Overseas Scholarship Award (TETFUND/ES/TSAS/MOU/FARA/2024/VOL.1) and computational resources from the Computational Materials Laboratory, Department of Pure and Applied Science, Ladoke Akintola University of Technology, Ogbomoso, Nigeria.

ORCID

Akeem Adekunle Adewale: 0000-0001-8768-3876
AbdulRaheem Abdulganiyu: 0009-0002-5340-1222
Kamaldeen Olasunkanmi Suleman: 0000-0002-9103-1974
Surajudeen Otolowo Azeez: 0000-0001-5737-1388
ISMAILA TAIWO Bello: 0000-0002-1109-9259
Yekinni Kolawole Sanusi: 0000-0001-6259-1166
De Conti Claudio: 0000-0002-3024-2671

Reference

[1] Suleman, K., Adewale, A., Azeez, S., Oladunni, S., Amuda, D., Ojuolape, A., Sanusi, Y., De Conti, C., Structural, electronic and optical properties of doped tio2: A first principle investigation. *Dutse Journal of Pure and Applied Sciences*, **2025**, 11(2d), 136–149.
[2] Wang, C., Wang, S.-J., Kong, F.-G., Calixarene-protected titanium-oxo clusters and their photocurrent responses and photocatalytic performances. *Inorganic Chemistry*, **2021**, 60(7), 5034–5041.
[3] Kang, X., Liu, S., Dai, Z., He, Y., Song, X., Tan, Z., Titanium dioxide: From engineering to applications. *Catalysts*, **2019**, 9(2), 191.
[4] Bhat, D.K., Bantawal, H., Uma, P., Kumar, S.P., Shenoy, U.S., Designing sustainable porous graphene-catio3 nanocomposite for environmental remediation. *Sustainable Chemistry for the Environment*, **2024**, 5, 100071.
[5] Passi, M., Pal, B., A review on catio3 photocatalyst: Activity enhancement methods and photocatalytic applications. *Powder Technology*, **2021**, 388, 274–304.
[6] Guo, X., Li, Y., Xiao, W., Wu, H., First-principles study on the electronic structure and optical properties of orthorhombic catio3 under different pressures. *Physica C: Superconductivity and its Applications*, **2024**, 617, 1354447.
[7] Y, Wang., J, Niu., Z, Zhang., X, Long., Sono-photocatalytic degradation of organic pollutants in water. *Progress in Chemistry*, **2008**, 20(10), 1621–1627.
[8] Ghazanfar, M., Azam, S., Nasir, M.F., Goumri-Said, S., Alrobei, H., Insight into electronic and optical properties of eu+ 2-doped catio3 from gga+ u calculations. *Journal of Solid State Chemistry*, **2021**, 293, 121796.
[9] Adewale, A.A., Chik, A., Adam, T., Yusuff, O.K., Ayinde, S.A., Sanusi, Y.K., First principles calculations of structural, electronic, mechanical and thermoelectric properties of cubic atio3 (a= be, mg, ca, sr and ba) perovskite oxide. *Computational Condensed Matter*, **2021**, 28, e00562.
[10] Ye, W., Zhu, C., Xiao, Y., Bai, X., Zheng, P., Zhang, J., Bai, W., Fan, Q., Zheng, L., Zhang, Y., Remarkable energy-storage performances and excellent stability in catio3-doped bifeo3-batio3 relaxor ferroelectric ceramics. *Journal of the European Ceramic Society*, **2023**, 43(3), 900–908.
[11] Rahaman, M., M. Kamruzzaman, ma helal, ie ara, akm farid ul islam &., A comparative study based on the first principles calculations of ATiO3 (A = Ba, Ca, Pb and Sr) perovskite structure. *Indian Journal of Physics*, **2016**, 90, 1105–1113.
[12] Saha, S., Sinha, T., Mookerjee, A., First principles study of electronic structure and optical properties of catio3. *The European Physical Journal B-Condensed Matter and Complex Systems*, **2000**, 18(2), 207–214.
[13] Yue, H., Fang, K., Chen, T., Jing, Q., Guo, K., Liu, Z., Xie, B., Mao, P., Lu, J., Tay, F.E.H., First-principle study on correlate structural, electronic and optical properties of ce-doped batio3. *Crystals*, **2023**, 13(2), 255.
[14] Boudali, A., Abada, A., Khodja, M.D., Amrani, B., Amara, K., Khodja, F.D., Elias, A., Calculation of structural, elastic, electronic, and thermal properties of orthorhombic catio3. *Physica B: Condensed Matter*, **2010**, 405(18), 3879–3884.
[15] Tahiri, O., Kassou, S., El Mrabet, R., Belaaraj, A., First principles calculations of electronic and optical properties for mixed perovskites: Ba (1-x) ca (x) tio 3 and ba (1-x) sr (x) tio 3 (x= 0.4, 0.6). *Materials and Devices*, **2018**, 3, 2004 (2018).

[16] Blaha, P., Schwarz, K., Tran, F., Laskowski, R., Madsen, G.K., Marks, L.D., Wien2k: An apw+ lo program for calculating the properties of solids. *The Journal of Chemical Physics*, **2020**, 152(7).
[17] Takeda, T., Kubler, J., Linear augmented plane wave method for self-consistent calculations. *Journal of Physics F: Metal Physics*, **1979**, 9(4), 661.
[18] Tran, F., Blaha, P., Accurate band gaps of semiconductors and insulators<? Format?> with a semilocal exchange-correlation potential. *Physical Review Letters*, **2009**, 102(22), 226401.
[19] Tao, J., Perdew, J.P., Staroverov, V.N., Scuseria, G.E., Climbing the density functional ladder: Nonempirical meta–generalized gradient approximation designed for molecules and solids. *Physical Review Letters*, **2003**, 91(14), 146401.
[20] Birch, F., Finite elastic strain of cubic crystals. *Physical Review*, **1947**, 71(11), 809.
[21] Tariq, S., Ahmed, A., Saad, S., Tariq, S., Structural, electronic and elastic properties of the cubic catio3 under pressure: A dft study. *Aip Advances*, **2015**, 5(7).
[22] Kurboniyon, M.S., Zafari, U., Ma, C.-G., Piasecki, M., Brik, M.G., Yamamoto, T., Geometrical and electronic structure analysis of mn-doped camo3 (m= ti, zr, and sn). *physica Status Solidi (b)*, **2023**, 260(9), 2200575.
[23] Cao, R., Fu, T., Xu, H., Luo, W., Peng, D., Chen, Z., Fu, J., Synthesis and luminescence enhancement of catio3: Bi3+ yellow phosphor by codoping al3+/b3+ ions. *Journal of Alloys and Compounds*, **2016**, 674, 51–55.
[24] Minagawa, K., Nishiguchi, Y., Oka, R., Masui, T., Synthesis and Characterization of Ca1- xEuxZrO3as Environmentally Friendly Inorganic Yellow Pigments. *ACS Omega*,**2021**, 6(4), 3411–3417.
[25] Zhu, A., Wang, J., Zhao, D., Du, Y., Native defects and pr impurities in orthorhombic catio3 by first-principles calculations. *Physica B: Condensed Matter*, **2011**, 406(13), 2697–2702.
[26] Boutinaud, P., Pinel, E., Dubois, M., Vink, A., Mahiou, R., Uv-to-red relaxation pathways in catio3: Pr3+. *Journal of Luminescence*, **2005**, 111(1-2), 69–80.
[27] Ueda, K., Yanagi, H., Noshiro, R., Hosono, H., Kawazoe, H., Vacuum ultraviolet reflectance and electron energy loss spectra of. *Journal of Physics: Condensed Matter*, **1998**, 10(16), 3669.
[28] Rosa, I.L.V., Oliveira, M., Assis, M., Ferrer, M., André, R., Longo, E., Gurgel, M.F., A theoretical investigation of the structural and electronic properties of orthorhombic cazro3. *Ceramics International*, **2015**, 41(2), 3069–3074.
[29] Adewale, A.A., Chik, A., Yusuff, O.K., Ayinde, S.A., Sanusi, Y.K., First principle calculation of structural, electronic and optical properties of cds and doped cdx-1axs (a= co, fe, ni) compounds. *Materials Today Communications*, **2021**, 26, 101882.
[30] Krause, A., Weber, W., Pohl, D., Rellinghaus, B., Kersch, A., Mikolajick, T., Investigation of band gap and permittivity of the perovskite catio3 in ultrathin layers. *Journal of Physics D: Applied Physics*, **2015**, 48(41), 415304.
[31] Piskunov, S., Heifets, E., Eglitis, R., Borstel, G., Bulk properties and electronic structure of srtio3, batio3, pbtio3 perovskites: An ab initio hf/dft study. *Computational Materials Science*, **2004**, 29(2), 165–178.
[32] Abraham, B.M., Yedukondalu, N., Vaitheeswaran, G., "Structural, electronic and lattice dynamical properties of perovskite CaZrO3 under high pressure," in *AIP Conference Proceedings*, **2017**.
[33] Chen, Z., Zhang, P., Chen, D., Wu, Y., Wang, M., Ma, N., Wang, H., First-principles investigation of thermodynamic, elastic and electronic properties of al3v and al3nb intermetallics under pressures. *Journal of Applied Physics*, **2015**, 117(8).
[34] Rekab-Djabri, H., Salam, M.M.A., Daoud, S., Drief, M., Guermit, Y., Louhibi-Fasla, S., Ground state parameters, electronic properties and elastic constants of camg3: Dft study. *Journal of Magnesium and Alloys*, **2020**, 8(4), 1166–1175.
[35] Ma, Y., Fo, Y., Wang, M., Liang, X., Dong, H., Zhou, X., Exploring the mechanism of ta3n5/ktao3 photocatalyst for overall water splitting by first-principles calculations. *Journal of Energy Chemistry*, **2021**, 56, 353–364.
[36] Mayengbam, R., Tripathy, S., Palai, G., First-principle insights of electronic and optical properties of cubic organic–inorganic mage x pb (1–x) i3 perovskites for photovoltaic applications. *The Journal of Physical Chemistry C*, **2018**, 122(49), 28245–28255.

Copyright © 2025 by authors and SPC (Sami Publishing Company) + is an open access article distributed under the Creative Commons Attribution License(CC BY) license،which permits unrestricted use, distribution, and reproduction in any medium, provided the original work is properly cited.